Applied Catalysis B: Environmental 197 (2016) 206–213

Contents lists available at ScienceDirect

Applied Catalysis B: Environmental

journal homepage: www.elsevier.com/locate/apcatb

Ce-promoted Ni/SBA-15 catalysts for anisole hydrotreating under mild conditions

Yongxing Yang[a,1], Cristina Ochoa-Hernández[a,2], Patricia Pizarro[a,b], Víctor A. de la Peña O'shea[a], Juan M. Coronado[a,*], David P. Serrano[a,b]

[a] Thermochemical Processes Unit, IMDEA Energy Institute, Avenida Ramón de la Sagra 3, Móstoles, 28935 Madrid, Spain
[b] Chemical and Environmental Engineering Group, ESCET, Rey Juan Carlos University, C/Tulipán s/n, Móstoles, 28933 Madrid, Spain

ARTICLE INFO

Article history:
Received 26 October 2015
Received in revised form
30 December 2015
Accepted 1 January 2016
Available online 6 January 2016

Keywords:
Bio-oil
Ce promoter
SBA-15
Selective hydrogenation
Aromatic hydrocarbons
Hydrotreating

ABSTRACT

Ce-containing SBA-15 materials with Ce/Si molar ratio ranging from 0 to 0.08 were prepared by mixing an acidic suspension of colloidal CeO_2 particles along with the surfactant during the synthesis of mesostructured silica. The obtained solids were characterized by powder X-ray diffraction (XRD), N_2 sorption isotherms, TEM, UV–vis, and Raman spectroscopy. Structural analyses confirmed that all the samples present a well-ordered hexagonal mesoporous structure, with larger pore diameter and volume than unmodified SBA-15 due to the incorporation of the lanthanide promoter. According to the characterization results different cerium species, namely dispersed Ce species and CeO_2 crystallites, are formed depending on the Ce/Si ratio of the Ce-SBA-15 materials. On the other hand, Ni/Ce-SBA-15 catalysts were prepared by wet impregnation of the mesoporous supports and the comparison of the different samples showed that the incorporation of Ce progressively enhances Ni dispersion. These catalysts were assayed for hydrotreating of anisole at temperatures in the 270–290 °C range and moderate hydrogen pressure (7 bar). Such process is relevant for the upgrading of bio-oils derived from the pyrolysis of lignocellulosic biomass. Catalytic activity tests reveal that conversion of anisole progressively improves with increasing Ce/Si ratio and exceeds 30% at 290 °C for the catalyst with Ce/Si = 0.08. In these conditions the main product is methoxycyclohexane in all cases. However, almost a two-fold increment of benzene yields can be obtained with Ce-promoted catalysts when compared to Ni/SBA-15. This enhancement of the selectivity towards aromatic is very promising for the development of a green route for the production of those chemicals.

1. Introduction

Bio-oils derived from the pyrolysis of lignocellulosic biomass contain high percentage of oxygen (45–50 wt%) due to the presence of oxygenated molecules such as guaiacols, phenols, furans, carboxylic acids, ketones, and levoglucosan among many others chemicals. These functionalized molecules are responsible for the undesirable properties of this liquid product, such as high viscosity, poor stability, acidity, limited heating value and low immiscibility of the bio-oils with fossil fuels [1,2]. In order to obtain hydrocarbon-based fuels, oxygen can be removed from the bio-oil using hydrogen at high pressure via a process known as hydrodeoxygenation (HDO) [2–10]. This upgrading process was initially performed using traditional hydrodesulfuration catalysts based on Ni, Co and Mo sulfides supported on Al_2O_3, which are successfully used for sulfur elimination from crude oils. Although these catalysts are also very active for oxygen removal, Al_2O_3 support is well known to promote coke formation, and the stability of the active sulfides is not adequate for processing biomass, which does not contain significant amount of sulfur [3]. Other catalysts based on supported noble metals, such as Rh [3], Ru [4], Pd [5] or Pt [6] can be very active for deoxygenation of molecules representative of bio-oils like guaiacol or anisole. Besides, catalysts based on Ni phosphides as active phases have been successfully applied for the hydrodeoxygenation of biomass derived chemicals as a convenient lower cost alternative to precious metals [7]. On the other hand, the development of more efficient bifunctional HDO catalysts by combining acidic supports with transition metal centers with hydrogenation capacity, such Ni or Co, can be very advantageous to modulate the selectivity and to optimize the hydrogen consumption by promoting the synergies between the different components

* Corresponding author.
E-mail address: juanmanuel.coronado@gmail.com (J.M. Coronado).
[1] Current address: Institute of Coal Chemistry, Chinese Academy of Sciences, Taiyuan, Shanxi, PR China.
[2] Current address: J. Heyrovský Institute of Physical Chemistry, Academy of Sciences of the Czech Republic, v.v.i., Dolejškova 3, Prague 8, 18223, Czech Republic.

http://dx.doi.org/10.1016/j.apcatb.2016.01.001
0926-3373/

of the catalysts [8–10]. Despite this progress, the development of HDO catalysts with even better performance is still a topic of great interest, as to overcome the numerous challenges of dealing with highly oxygenated bio-oils as feedstock.

Ordered mesoporous silicas, such as SBA-15, are very suitable catalyst's support for dispersing a number of active phases, because its network of uniform and relatively large pores facilitates interactions with bulky molecules. Accordingly, catalysts based on SBA-15 have been often applied to HDO of different bio-liquids [11–13]. In order to further improve the reactivity of these materials, incorporation of other elements in the siliceous structure has been frequently attempted [13]. Among these promoted mesoporous materials, Ce-containing silica have been tested in processes such as alcohol reforming or selective hydrogenation because this rare-earth element is a well-known catalytic promoter [14–17]. Preparation of Ce-SBA-15 has been approached via a sol–gel route [15], or in a two-step synthesis method in acid media by controlling the pH [16]. Corma et al. synthesized mesostructured silica with high specific surface areas using 4 nm CeO_2 nanoparticles prepared separately as precursor. After loading Pt on these Ce-modified support, the resulting catalyst showed the largest activity and selectivity for the hydrogenation of crotonaldehyde to crotyl alcohol [17].

Despite this potential for modulating product distribution, to the best of our knowledge, the use Ce-SBA-15 as an alternative support for promoting hydrodeoxygenation of biomass derived molecules has not been previously explored. In the present work, the performance of Ni/Ce-SBA-15 catalysts with different content of this lanthanide was studied for the HDO of anisole, which can be considered a representative chemical of bio-oils composition. With this aim, a series of Ce-SBA-15 materials with low Ce/Si molar ratio (0-0.08) were successfully synthesized under strong acidic conditions using a commercial colloidal CeO_2 suspension as Ce source. In this method, the assembly process was controlled by adjusting the interactions of a copolymer template with the ceria nanoparticles and the SiO_2 sol. In order to ascertain the nature of cerium species present in the mesoporous silica matrix, all the samples were characterized by XRD, N_2 sorption, TEM, and UV–vis and Raman spectroscopy. The results obtained confirm the superior catalytic activity and selectivity towards aromatic products of Ce-contained catalyst, as compared with a similarly prepared sample based on pure silica SBA-15.

2. Experimental

2.1. Materials

Ce-SBA-15 supports were synthesized using as a precursor a colloidal acidic suspension of CeO_2 nanoparticles (Sigma–Aldrich, 10 wt% in H_2O), which was incorporated during the formation of mesostructured silica following the method described elsewhere [17]. The pH of the suspension of ceria nanoparticles was adjusted by adding different amounts of HCl to get a final concentration ranging from 0.5 to 2 M, and then it was mixed with an aqueous solution of polyalkylene oxide block copolymer (Pluronic P123, Sigma-Aldrich). Then, TEOS (Sigma) was added into the dispersion at room temperature under continuous stirring for 1 h. The resulting suspension was kept at 45 °C for 16 h. The mixture was aged overnight at 80 °C without further stirring. The solid precipitate was recovered, washed with deionized water, and air-dried at 80 °C. The copolymer template was removed by slowly increasing the calcination temperature from 20 to 500 °C in 6 h, and keeping the sample at this temperature for 6 h.

Supported Ni (5 wt% Ni) catalysts were prepared by wet impregnation of the Ce-SBA-15 materials with an aqueous solution of $Ni(NO_3)_2{\cdot}6H_2O$ (Sigma). Subsequently, this sample was dried at 80 °C, and calcined in air at 450 °C for 4 h.

2.2. Characterization

XRD patterns of the supports and catalysts were recorded with a Philips PW 3040/00 X'Pert diffractometer using Cu Kα radiation operated at 45 kV and 40 mA.

Metal content was determined by ICP-OES on a Perkin Elmer Optima 7300AD instrument after digestion of the solid samples. TEM images of the materials were taken using a PHILIPS TECNAI 20T instrument, working at 200 kV and equipped with an EDX spectrometer for measuring X-ray energy dispersive data.

Textural properties were measured by N_2 adsorption-desorption experiments at 77 K on a Quadrasorb system (Quantachrom). The surface area was calculated using the B.E.T. equation, and the pore size distribution was estimated from the adsorption branch of the isotherm using the Barrett–Joyner–Halenda (BJH) method.

The reducibility of the catalyst precursors was determined by hydrogen temperature-programmed reduction (H_2-TPR), whereas acidity of the samples was determined by temperature programmed desorption of ammonia (NH_3-TPD). Both types of assays were performed in a Micromeritics AUTOCHEM 2910 equipment, loading 50-mg of sample in a quartz U-tube reactor. The TPR tests were conducted in a 10% H_2/Ar flow of 50 ml/min at a heating rate of 10 °C/min, and the hydrogen consumption was determined using a thermal conductivity detector (TCD).

Optical properties were measured in diffuse reflectance mode using $BaSO_4$ in a UV/Vis/NIR Perkin Elmer Lambda 1050 Spectrometer, and Raman spectra of the sample powder were acquired in atmospheric conditions using a JASCO NRS-5000/7000 series spectrometer.

The activity of the catalysts was studied in a fixed-bed tubular reactor (i.d. = 9 mm and l = 305 mm) with the catalyst bed placed upon a porous plate (Microactivity-Reference, PID Eng & Tech) operated at 7 bar and 290 °C, with a feedstock containing 4 wt% anisole (Aldrich) in heptane. About 200 mg of catalyst pelletized, crushed and sieved with 40–60 mesh, and then mixed with silicon carbide were used in the assays. Before reaction, the catalysts were reduced in situ with a flow of pure hydrogen (60 ml/min) at 550 °C. The hydrogen flow rate was 30 ml/min and the organic phase was introduced at a rate of 48 ml/h, corresponding to a space velocity of 163.2 h^{-1}, respectively. Liquid samples collected at 1 h intervals were analyzed off-line by gas chromatograph (Agilent, 7890A) equipped with a flame ionization (FID) detector and a HP-INNOWAX column for product analysis.

3. Results and discussion

3.1. Effect of acid concentration on the synthesis of Ce-SBA-15

In order to determine the most adequate conditions for preparing Ce-SBA-15 supports, the effect of pH on the formation of these mesostructures was first studied by keeping constant other synthesis parameters. With this aim, the acidity of the reaction media was varied by adding different amounts of concentrated HCl to the aqueous suspension of CeO_2 before the surfactant P123 was dissolved. Fig. 1A shows the low angle XRD patterns of the Ce-SBA-15 samples synthesized using HCl concentrations varying from 0.5 to 2 M, and fixing the initial Ce/Si = 0.05. All the XRD patterns show three well-resolved peaks at (1 0 0), (1 1 0) and (2 0 0) that are indicative of highly ordered mesoporous structures [18]. The final Ce/Si ratio of the Ce-SBA-15 samples strongly depends on the acidic environment used during the synthesis, which control the partial dissolution of

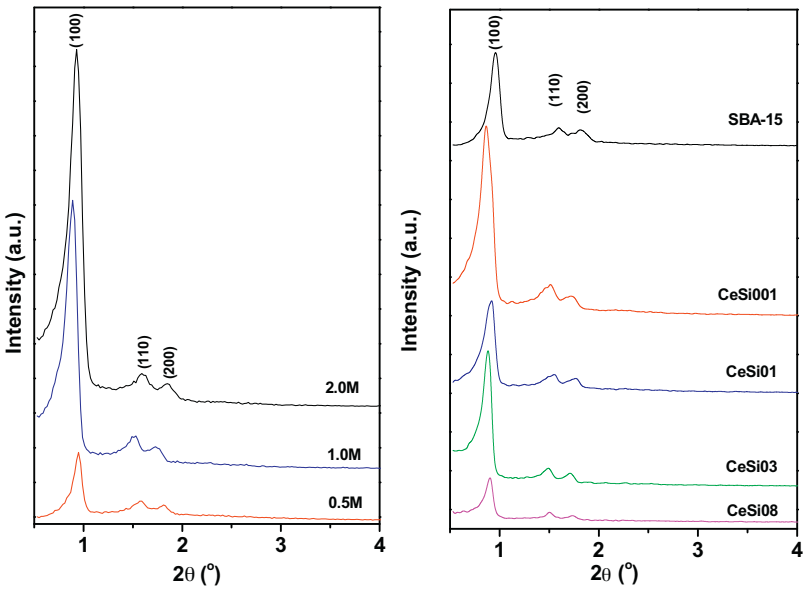

Fig. 1. Low-angle XRD patterns of Ce-SBA-15synthesized at (A) different acidic condition and (B) by changing the Ce/Si ratio.

CeO_2 colloidal particles. Thus, using strong acidic condition (2 M) and an initial Ce/Si molar ratio of 0.05, chemical analysis reveals that Ce is not incorporated into the SBA-15. In contrast, samples synthesized in 1 M and 0.5 M solutions of HCl present a final Ce/Si ratio in the solid products of 0.005 and 0.03, respectively. Therefore, it can be concluded that weaker acidic media makes the Ce incorporation easier, the amount of this lanthanide in the final material being progressively higher with increasing the pH.

Accordingly, Ce-SBA-15 catalysts' supports with different Ce/Si ratio, as discussed in detail in the following sections, were subsequently prepared using 0.5 M HCl solutions.

3.2. Effect of Ce/Si ratio on the physicochemical properties of the Ce-SBA-15 supports

Ce-SBA-15 samples with different Ce/Si ratio synthesized in 0.5 M HCl were characterized using different techniques. Fig. 1B displays the low angle XRD patterns of all these solids, which in all cases present three well-resolved peaks assigned to the (1 0 0), (1 1 0) and (2 0 0) reflections of a p6mm hexagonal array of parallel channels. These profiles are analogous to those of pure silica SBA-15 and confirm the formation of mesostructured materials. Nevertheless, the progressive decrease in the intensity of the low angle XRD pattern with increasing the Ce content reveals a gradual loss of long range order of SBA-15. In addition, as it can be observed in Table 1, the unit cell parameters, a_0, of all the Ce-SBA-15 samples (varying between 11.0–11.7 nm) is larger than that (10.6 nm) of pure silica SBA-15. This enlargement of the cell parameters has been previously observed in Ce-modified mesostructured silica prepared form soluble precursors and, as in the present case, no obvious correlation between the amount of Ce and the dimensions of the lattice can be found [19]. For these samples prepared from colloidal suspension, most likely these variations reflect the changes induced by CeO_2 nanoparticles during the gel formation, as it will be discussed below.

Fig. 2 shows the high angle XRD patterns of Ce-SBA-15 samples with different Ce/Si ratio. Four well-resolved diffraction peaks are observed at 28.6°, 33.1°, 47.5° and 56.3°, corresponding respectively to (1 1 1), (2 0 0), (2 2 0) and (3 1 1) planes of cubic CeO_2 with fluorite structure (Fm3m, JCPDS: 43–1002), except for the sample with Ce/Si = 0.001. As expected, these reflections become gradually

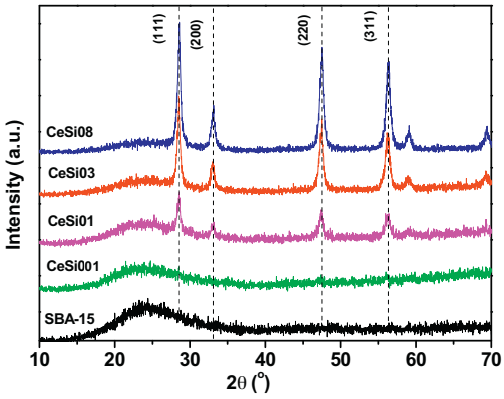

Fig. 2. High-angle XRD patterns of Ce-SBA-15synthesized with different Ce/Si molar ratio.

sharper and more intense with increasing the amount of cerium and these results indicate the formation of CeO_2, which according to the size estimated from Scherrer equation should lay outside the silica channels. Likewise, the diameter of theses ceria crystallites increases with the Ce/Si ratio (Table 1). Finally, it can be noticed that the very broad peak centered at around 22 can be attributed to the amorphous nature of the silica walls and, accordingly, it is more intense for the Ce-free SBA-15 sample used as reference.

Table 1 collects the textural parameters obtained from the N_2 adsorption isotherms of the different Ce-SBA-15 samples. All the isotherms correspond to type IV with H1 hysteresis loop, which is typical of mesoporous materials with 2D hexagonal structure and a narrow pore size distribution [17,18]. The well-defined step which occurs at relative high pressure of 0.6–0.8, corresponding to capillary condensation of N_2, also reveals the uniformity of the pores (see SI Fig. 1). With the introduction of cerium, the onset of the capillary step for the Ce-SBA-15 samples shift to higher relative pressure. This fact reflects an increase in the mesopore diameter as it has been observed in other metal-modified SBA-15 [19]. The BJH pore size distribution also confirms that all the Ce-SBA-15 samples possess uniform mesopore pore diameter of ca. 9 nm which is larger than those of pure silica SBA-15. These data also indicate that pore diameters are slightly enlarged with increasing Ce/Si ratio, allowing certain tuning of the pore dimensions by varying the

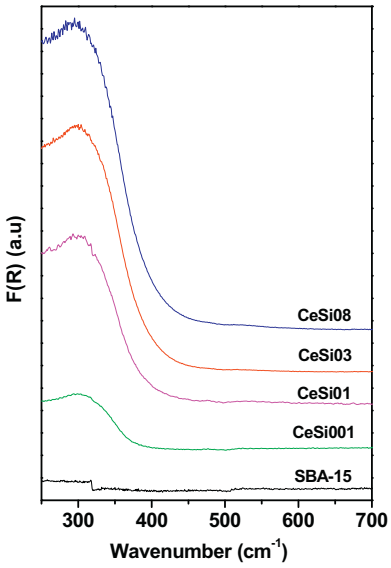

Fig. 3. UV–vis diffuse reflectance spectra of Ce-SBA-15synthesized with different Ce/Si molar ratios.

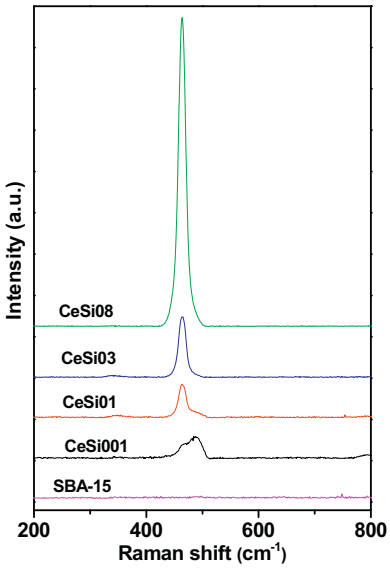

Fig. 4. Raman spectra of Ce-SBA-15synthesized with different Ce/Si molar ratios.

content of cerium. In addition, it is also worth pointing out that the Ce-SBA-15 samples with Ce/Si = 0.001–0.03 display much higher surface area and total pore volume than pure silica SBA-15 (see Table 1). On the other hand, the walls thickness is lower for the Ce-containing samples, as it can be observed in Table 1. Generally, addition of inorganic salts could lead to micelles with larger diameter, which results in the increase in pore diameter and help to obtain highly ordered mesoporous materials due to the specific interaction between non-ionic surfactant and metal ions [18,20–22]. In the present case, ceria nanoparticles (or cerium ions originated from partly dissolved ceria) can lead to a similar salt effect. Hence, this synthesis method not only introduces cerium into SBA-15, but it also helps to improve the properties of SBA-15 in terms of pore diameter and volume (as shown in Table 1), at expenses of thinner walls of the mesostructure. However, it is worth noting that for larger Ce content a progressive decrease of surface area and pore volume is observed, which suggest a certain blockage of the channels by the promoter

TEM images of Ce-SBA-15 (see SI Fig. 2) confirm the formation of well-ordered hexagonal arrays of mesopores with one-dimensional channels, which is arranged in a 2D hexagonal mesostructure. TEM and EDX analyses results also reveal the presence of some aggregates of ceria nanoparticles of about 20–50 nm unevenly distributed mainly outside the channels. The presence of these extra-framework CeO_2 agglomerates observed in the external surface is consistent with the XRD, which suggest the formation of crystallites larger than the pore diameter.

Fig. 3 shows UV–vis diffuse reflectance spectra of Ce-SBA-15 samples with different Ce/Si ratio. All the Ce-SBA-15 samples present a large absorption at ca. 300 nm, which can be ascribed to the ligand to metal charge transfer transition of Ce^{4+}-O^{2-} centers of well-dispersed cerium species [23]. These centers may correspond to both Ce^{4+} ions isolated inside the silica matrix or to small surface CeO_2 clusters. The progressive enhancement of the intensity at ca. 300 nm with increasing cerium content suggests that a substantial fraction of this lanthanide oxide is dispersed in the SBA-15 matrix at the selected Ce/Si ratios using this synthesis route. However, the contribution of larger CeO_2 crystallites to the UV–vis spectra does not seem to be important because, for these species the absorption edge starts at about 420 nm [23] and, even for the samples with higher Ce/Si content the intensity above 400 nm is very weak.

Fig. 4 shows the Raman spectra of the Ce-SBA-15 materials. For Ce/Si ratio larger than 0.005, all the Ce-SBA-15 samples present a prominent peak at about 463 cm^{-1}. This band corresponds to the F_{2g} phonon mode of the fluorite structure of CeO_2 [15]. Moreover, it is also observed that with increasing Ce concentration the Raman peak sharpens and becomes more symmetrical. This could be due to better crystallization of ceria at higher content, as observed from XRD measurements. In contrast, in the case of sample with the lower Ce content, the spectrum displays a broader and asymmetric band with a shoulder at about 460 cm^{-1} and a maximum at about 490 cm^{-1}. A similar feature at high wavenumber was reported on Ce-SBA-15 sample prepared by impregnation using organometallic precursors [24], and it can be attributed to Ce species in close interaction with the SiO_2 matrix.

Overall, characterization of Ce-SBA-15 samples reveals that the lanthanide promoter is present as both CeO_2 crystallites and more dispersed species. XRD and TEM indicate that crystallites are mainly

Table 1
Physicochemical properties of Ce-SBA-15 supports.

Samples' labels	Ce/Si molar ratio		a_0[a] (nm)	d_{CeO2}[b] (nm)	S_{BET} (m^2/g)	V_{total} (cm^3/g)	Pore diameter D_p (nm)	Wall thickness[c] w (nm)
	Gel	Solid						
SBA-15	0	0	10.6		739	0.75	7.1	3.5
CeSi-001	0.01	0.001	11.7		896	1.19	9.3	2.4
CeSi-01	0.02	0.01	11.0	11	876	1.13	8.8	2.2
CeSi-03	0.05	0.03	11.4	20	782	1.06	9.1	2.3
CeSi-08	0.10	0.08	11.2	25	696	0.98	9.3	1.9

[a] a_0: Unit cell parameter, $a_0 = 2d(1\,0\,0)/3^{1/2}$.
[b] Determined from Scherrer equation using the width at half height of the (1 1 1) reflection of CeO_2.
[c] $w = a_0 - D_p$.

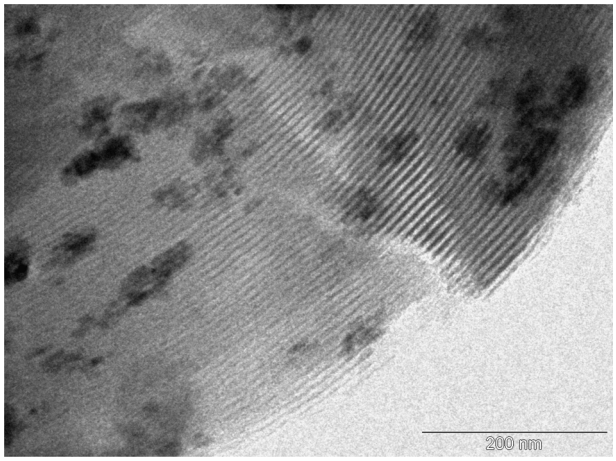

Fig. 5. TEM image of the5% Ni/Ce-SBA-15 catalysts with Ce/Si = 0.03.

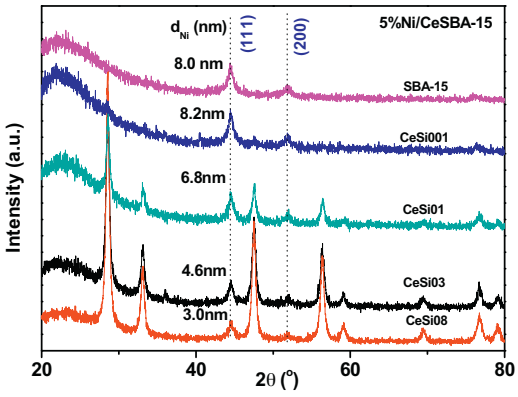

Fig. 6. High-angle XRD patterns of 5% Ni/Ce-SBA-15 catalysts prepared with different Ce/Si molar ratio.

located evenly in the external surface of SBA-15. Likewise, dispersed Ce moieties, although can be predominant at low Ce/Si, as Raman spectra suggest, are also present a significant proportion at higher Ce/Si, as the UV–vis spectra point out.

3.3. Characterization of the Ni/Ce-SBA-15 catalysts

In order to provide hydrogenation activity for biomass deoxygenation the Ce-SBA-15 supports were impregnated with 5 wt% of Ni. Textural properties of these catalysts are summarized in Table 2. Overall, the incorporation of the metal phase, results in a significant decrease of surface area and pore volume, which cannot be justified only by the slightly lower proportion of the mesoporous support. These results indicate that Ni particles are incorporated into the channels causing a partial blocking. This is consistent with the TEM study, as it can be observed in the image of Fig. 5, which shows irregularly distributed areas of dark contrast, mainly with elongated shape. EDX (see SI Fig. 3) also confirms the simultaneous presence of Ce and Ni on SBA-15 support. On the other hand, it seems that the reduction of textural properties upon Ni incorporation is more significant in the case of the samples with lower Ce content. In contrast, pore diameter decreases appreciably more for catalyst with larger Ce content.

Fig. 6 displays the high angle XRD patterns of the Ni/Ce-SBA-15 catalysts after reduction in hydrogen at 550 °C. In addition to the features corresponding to amorphous SiO_2 and CeO_2, which are also present in the XRD plot of Fig. 2, additional reflections due to the formation of Ni° crystallites (JCPDS: 04-0850) are observed for these catalysts. Interestingly, the peaks corresponding to the metal phase

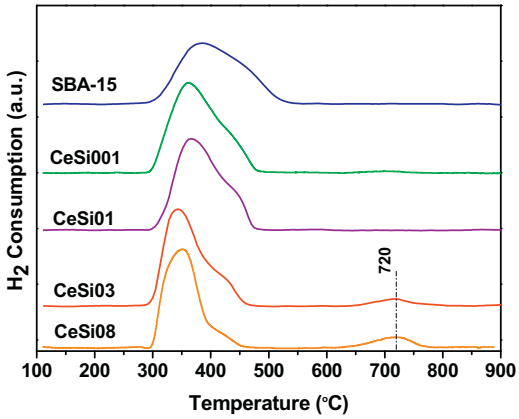

Fig. 7. H_2-TPR profiles of the 5% Ni/Ce-SBA-15 catalysts with different Ce/Si molar ratio.

are much sharper for the samples with lower Ce content. Therefore, the size of Ni nanocrystallites progressively decreases with the addition of this lanthanide (see Table 2). Similar results have been reported for Ni/Ce-SBA-15 applied to dry reforming of methane [25]. Thus, for the catalysts with Ce/Si = 0.08 the average diameter of Ni particles is 3 nm, whereas for the pure siliceous SBA-15 is 8 nm. An estimation of the metal dispersion can be calculated from the Ni crystallite sizes using the equations described elsewhere [26], and the obtained values are summarized in Table 2. These results reveal the positive effect of Ce-incorporation for improving the dispersion of metallic Ni, which shows a two-fold increment by increasing the Ce/Si ratio from 0.01 to 0.08. This observation can be related, at least partly, to the improved textural properties of the Ce-promoted catalysts, such as larger pore diameter, but the intensity of the effect suggests that it may be also favored by a specific interaction between Ni and CeO_2.

Fig. 7 shows the H_2-TPR profiles of the calcined precursors of the 5 wt% Ni/Ce-SBA-15 catalysts with different Ce content. In the case of Ce-free Ni/SBA-15 sample a broad an asymmetric reduction peak with a maximum at around 382 °C, arising from the reduction of bulk NiO to Ni°, can be observed. This broad reduction event suggests a rather heterogeneous distribution of metal particles on the siliceous support, in such a way that NiO crystallites with higher interaction with the silica will be reduced at higher temperature. The influence of cerium species on the reduction of NiO is clear for all NiO/Ce-SBA-15 materials, because the reduction peaks become narrow with increasing the Ce content and shift to lower temperature. Thus, the maximum of the reduction event of NiO for the sample with Ce/Si = 0.001 is about 35 °C lower than for NiO/SBA-15, suggesting that the presence of cerium species could significantly promote the reducibility of the active metal even at low concentration, as it has been previously reported [25]. Further displacement to lower temperatures is observed for the samples high Ce/Si, which can be due to the proximity of NiO crystallites to CeO_2 particles. Although the asymmetry of the TPR peaks points out to the existence of different degrees of interactions between the different phases, the narrowing of the peaks for the samples with high Ce/Si suggest that specific interaction between the metal and the promoter are predominant for these samples. Thus, the close vicinity of Ni and Ce components, as it also suggested by the EDX analysis, is beneficial for the reducibility of Ni/Ce-SBA-15 catalysts. Finally, it should be mention that the weak feature at 720 °C can be attributed to the surface reduction of Ce^{4+} to Ce^{3+} species of very small CeO_2 oxide crystallites or dispersed Ce phases, confirming the presence of these moieties at high Ce/Si ratio.

In summary, it can be concluded that, despite the heterogeneity of the Ni/Ce-SBA-15 catalysts, evidences of the interaction between

Table 2
Physicochemical properties of 5% Ni/Ce-SBA-15 catalysts.

Catalysts	Ce/Si molar ratio	d_{Ni}[a] (nm)	S_{BET} (m^2/g)	V_{total} (cm^3/g)	Pore diameter D_p (nm)	Metal Dispersion D (%)[b]
Ni/SBA-15	0	8.0	594	0.67	6.7	15.5
Ni/CeSi-001	0.001	8.2	624	0.80	8.0	15.2
Ni/CeSi-01	0.01	6.8	518	0.71	8.0	18.3
Ni/CeSi-03	0.03	4.6	637	0.83	8.3	24.8
Ni/CeSi-08	0.08	3.0	603	0.77	7.4	31.1

[a] Determined from Scherrer equation using the width at half height of the (1 1 1) reflection of Ni°.
[b] Estimated from d_{Ni} using the equations derived in [26].

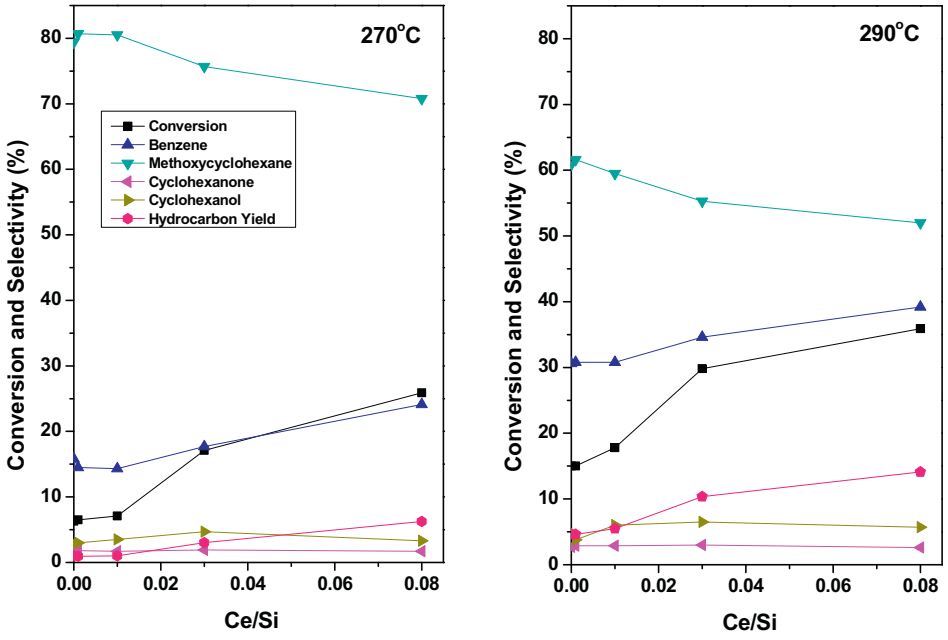

Fig. 8. Effect of Ce/Si molar ratio on the anisole hydrotreating conversion and selectivity over 5% Ni/Ce-SBA-15 catalysts at 270 and 290 °C. Reaction conditions: 7 bar, WHSV: 163.2 h^{-1}, H_2/feedstock ratio: 300 $Nm^3\ m^{-3}$, after 6 h on stream.

Ni and Ce components are provided by TPR, suggesting that Ni characteristics are affected by the both CeO_2 crystallites and more dispersed Ce species.

3.4. Performance of Ni/Ce-SBA-15 catalysts for anisole hydrotreating

Methoxyphenols are among the most abundant oxygenated compounds in bio-oils obtained from lignocellulose. Accordingly, anisole (methoxybenzene) was chosen as an adequate model compound to evaluate the catalytic properties of Ni/Ce-SBA-15 samples for hydrotreating biomass derived feedstocks. Fig. 8 displays the performance of the catalyst with different Ce/Si content at two different operation temperatures (270 and 290 °C) and using a relatively low hydrogen pressure (7 bar). These results indicate that the Ni/Ce-SBA-15 catalyst with Ce/Si = 0.001 presents a very similar activity to the catalyst based on pure silica mesoporous support. However, when Ce content further increases the conversion improves significantly. This observation suggests that CeO_2 crystallites rather than well-dispersed Ce-species are more efficient for promoting hydrotreating. In this way, the material with Ce/Si = 0.08 displays the maximum activity among all the samples, reaching a conversion of about 25%. This catalyst shows a three-fold and two-fold increment in the conversion at, respectively, 270 and 290 °C, in comparison with Ni/SBA-15 catalyst. Such enhanced performance with increasing Ce content can be attributed partly to the better Ni dispersion, which possibly contributes also to create new active sites in the interphase between the metal particles and the Ce-containing surface species. Turnover frequencies (TOF) for anisole conversion to benzene can be estimated from the Ni dispersion and they are collected in Table 3.

Table 3
Anisole hydrodeoxygenation over 5% Ni/Ce-SBA-15 catalysts.

Catalysts	Ce/Si molar ratio	Rate ($\mu mol/s\ g_{Cat.}$)		TOF[a] (s^{-1}) × 10^3	
		270 °C	290 °C	270 °C	290 °C
Ni/CeSi-001	0.001	0.22	0.50	1.3	5.8
Ni/CeSi-01	0.01	0.23	0.60	1.2	5.9
Ni/CeSi-03	0.03	0.54	0.97	2.4	7.9
Ni/CeSi-08	0.08	0.80	1.11	2.8	7.3

[a] For benzene production estimated from Ni dispersion.

Methoxycyclohexane and benzene are the main products of anisole hydrogenation over Ni/Ce-SBA-15 catalysts, but lower amounts of cyclohexanone, cyclohexanol, cyclohexane and phenol are also detected. A scheme of the possible hydrogenation routes of anisole is plotted in sFig. 9. Similar product distribution was found in previous reports using a variety of Ni supported catalysts under mild hydrotreating conditions [9,27–29]. As it can be appreciated in Fig. 8, Ce incorporation seems to promote the formation of benzene while decreasing the selectivity to methoxycyclohexane at the two temperatures used for the catalytic tests. Although these variations in the product distribution depend on the conversion degree, the influence of Ce on tuning the production of aromatics seems clear considering the relatively small variations in the degree of anisole transformation. On increasing the temperature to 290 °C,

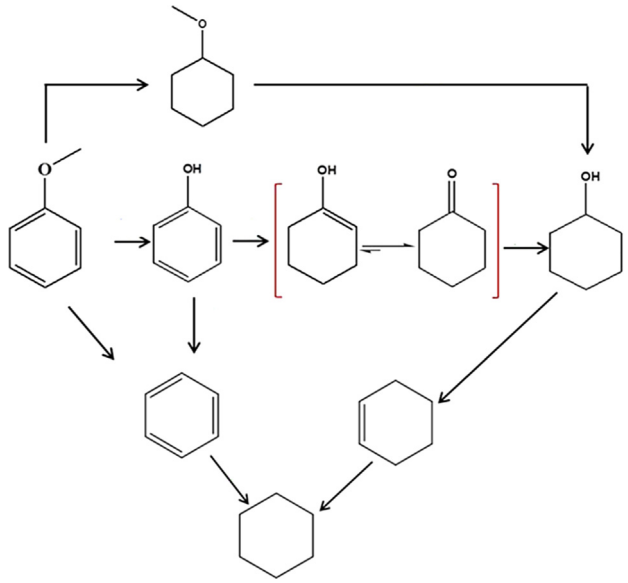

Fig. 9. Scheme of the transformation routes of anisole hydrotreating.

the activity is enhanced remarkably for all the catalysts and the promoting effect of Ce becomes more apparent. This fact indicates that higher temperatures favor the hydrogenolysis of methoxy group from anisole molecules, in larger extent than the hydrogenation of the aromatic ring. Turnover frequencies for anisole conversion to benzene (see Table 3) indicate that Ce promotion is more efficient for the catalysts with Ce/Si = 0.03 and slightly declines for higher lanthanide content. The activity of these catalysts for the production of aromatic is lower but comparable to that obtained with Mo_2C catalysts under milder conditions (150 °C and 1 bar) [28]. However, using this unsupported carbide a much higher selectivity to benzene can be achieved. On the other hand, a TOF as large as 0.85 s^{-1} can be obtained for the conversion of anisole at 70 °C and moderate pressure (4 bar) using a Pd/SiO_2 modified with Rh complexes, although in this case the main product is that of the oxygenation of the aromatic ring, methoxycyclohexane [29].

On the other hand, it is worth noting that under these conditions most of the products of anisole hydrogenation obtained over Ni/Ce-SBA-15 catalysts are still oxygenated molecules. Therefore an incomplete hydrodeoxygenation is achieved, with a maximum hydrocarbon yield of about 10%, which is much lower than that obtained with active phases such Mo_2C [28]. Accordingly, under these operation conditions this catalytic process appears more adequate for obtaining of chemicals, which could be further processed in a biorefinery scheme, than for the direct production of advanced biofuels.

Methoxycyclohexane results from the direct hydrogenation of the aromatic ring of anisole, which is expected to take place following the π-complex adsorption of this molecule on Ni particles. These surface complexes are more likely to form easily over larger Ni particles with well-ordered surface planes. On the contrary, smaller Ni particles as those existing over catalysts with high Ce content are expected to be less favorable for adsorption based of π-coordination, as this configuration require the participation concourse of several metal atoms. Therefore, increasing the Ce/Si ratio in the supports, the methoxycyclohexane selectivity would decrease gradually due to changes in the size of Ni crystallites and the structure sensitivity of this type of surface interactions [30]. On the other hand, benzene is formed by the direct hydrogenolysis of methoxy group of the anisole molecule. As mentioned above, benzene selectivity is enhanced with increasing Ce content. In this regards, the possible formation of active sites in the interface between Ni and CeO_2 moieties may favor the production of aromatics under mild hydrotreating conditions, as it has been reported previously for Ni/CeO_2 catalysts [9]. Other studies have found a promoting effect of Ce on the hydrodeoxygenation of cyclohexanone over Ni-W-B amorphous catalyst [31].

In summary, this study reveals that the better dispersion of the active metal over Ce-SBA-15 in comparison with unpromoted SBA-15, not only improve significantly the catalytic activity for hydrotreating, but also enhance the conversion of anisole to potentially valuable chemicals, such as benzene, under moderate hydrogen pressure and using renewable feedstocks. On this regards, it is worth noting that although a continuous improvement of the rate is observed for the whole range of compositions investigated, the effect is more remarkable at lower Ce content. In this way, Ce-promotion of aromatic yield is more efficient for the catalyst with a Ce/Si ratio of 0.03, as it is reflected in the corresponding TOF.

4. Conclusions

Ce-SBA-15 materials have been synthesized using commercially available colloidal CeO_2 nanoparticles directly incorporated during the formation of the gel. All the Ce-SBA-15 materials prepared in this way possess the ordered hexagonal mesoporous structure typical of SBA-15, but with slightly larger unit cell parameter. Furthermore, these materials present larger pore diameter, higher volume and thinner walls than the pure siliceous materials prepared at the same pH. The results of different characterization techniques indicate than on increasing Ce/Si, CeO_2 crystallites are formed, although a significant percentage of the lanthanide promoter remains in the form of well dispersed species. Impregnation of these modified supports with Ni results in an enhancement of the dispersion of this active metal, which seems to be correlated to Ce content. These Ni/Ce-SBA-15 catalysts show an improved catalytic activity for anisole hydrotreating, and better selectivity towards the production of benzene. Kinetic parameters indicate that Ce promotion is more efficient for intermediate Ce content (Ce/Si = 0.03). Enhancement of the performance of Ce-containing catalysts is probably related to the better dispersion of the metallic phase and to the formation of specific active sites in the Ni° particles in contact with Ce-containing surface species.

Acknowledgements

This study has received financial support of the RESTOENE-2 program funded by Consejería de Educación of Comunidad de Madrid and LIGCATUP from the Spanish Ministry of Economy and Competitiveness (ENE2011-29643-C02-01). YXY and VPO thank the financial support of, respectively, AMAROUT (European Commission) and "Ramón y Cajal" (MINECO) programs.

Appendix A. Supplementary data

Supplementary data associated with this article can be found, in the online version, at http://dx.doi.org/10.1016/j.apcatb.2016.01.001.

References

[1] G.W. Huber, S. Iborra, A. Corma, Chem. Rev. 106 (2006) 4044–4098.
[2] D.C. Elliott, T.R. Hart, Energy Fuels 23 (2009) 631–637.
[3] Y.-C. Lin, C.-L. Li, H.-P. Wan, H.-T. Lee, C.-F. Liu, Energy Fuels 25 (2011) 890–896.
[4] J. Wildschut, M. Iqbal, F.H. Mahfud, I.M. Cabrera, R.H. Venderbosch, H.J. Heeres, Energy Environ. Sci. 3 (2010) 962–970.
[5] Y.-K. Hong, D.-W. Lee, H.-J. Eom, K.-Y. Lee, Appl. Catal. B 150–151 (2014) 438–445.

[6] R.C. Runnebaum, T. Nimmanwudipong, D.E. Block, B.C. Gates, Catal. Lett. 141 (2011) 817–820.
[7] H.Y. Zhao, D. Lia, P. Buia, S.T. Oyama, Appl. Catal. A. 391 (2011) 305–310.
[8] A.R. Ardiyanti, S.A. Khromova, R.H. Venderbosch, V.A. Yakovlev, H.J. Heeres, Appl. Catal. B 117–118 (2012) 105–117.
[9] Y. Yang, C. Ochoa-Hernández, V.A. de la Peña O'Shea, P. Pizarro, J.M. Coronado, D.P. Serrano, Appl. Catal. B 145 (2014) 91–100.
[10] T.M. Sankaranarayanan, A. Berenguer, C. Ochoa-Hernández, I. Moreno, P. Jana, J.M. Coronado, D.P. Serrano, P. Pizarro, Catal. Today 243 (2015) 163–172.
[11] C.V. Loricera, B. Pawelec, A. Infantes-Molina, M.C. Álvarez-Galván, R. Huirache-Acuña, R. Nava, J.L.G. Fierro, Catal. Today 172 (1) (2011) 103–110.
[12] I.T. Ghampson, C. Sepúlveda, R. García, J.L.G. Fierro, N. Escalona, W.J. De Sisto, Appl. Catal. A 435–436 (2012) 51–60.
[13] C. Ochoa-Hernández, Y. Yang, P. Pizarro, V.A. de la Peña O'Shea, J.M. Coronado, D.P. Serrano, Catal. Today 210 (1) (2013) 81–88.
[14] J.A. Calles, A. Carrero, A.J. Vizcaíno, Microporous Mesoporous Mater. 119 (2009) 200–207.
[15] J.S. Li, Y.X. Hao, H.J. Li, M. Xia, X.Y. Sun, L.J. Wang, Microporous Mesoporous Mater. 120 (2009) 421–425.
[16] Q.G. Dai, X.Y. Wang, G.P. Chen, Y. Zheng, G.Z. Lu, Microporous Mesoporous Mater. 100 (2007) 268–275.
[17] P. Concepción, A. Corma, J. Silvestre-Albero, V. Franco, J.Y. Chane-Ching, J. Am. Chem. Soc. 126 (2004) 5523–5532.
[18] D. Zhao, Q. Huo, J. Feng, B.F. Chmelka, G.D. Stucky, J. Am. Chem. Soc. 120 (1998) 6024–6036.
[19] M.N. Timofeeva, S.H. Jhung, Y.K. Hwang, D.K. Kim, V.N. Panchenko, M.S. Melgunov, Y.A. Chesalov, J.-S. Chang, Appl. Catal. A 317 (2007) 1–10.
[20] Y. Wen, Y. Wang, J. Zhu, Adv. Mater. 15 (2003) 1943–1945.
[21] Y. Li, Z. Feng, Y. Lian, K. Sun, L. Zhang, G. Jia, Q. Yang, Microporous Mesoporous Mater. 100 (2007) 268–275.
[22] J.A. Hernández, S. Gómez, B. Pawelec, T.A. Zepeda, Appl. Catal. B 89 (1-2) (2009) 128–136.
[23] J.M. Coronado, A.J. Maira, A. Martıínez-Arias, J.C. Conesa, J. Soria, J. Photochem. Photobiol. A 150 (1–3) (2002) 213–221.
[24] J. Strunk, W.C. Vining, A.T. Bell, J. Phys. Chem. C 115 (10) (2011) 4114–4126.
[25] N. Wang, W. Chu, T. Zhang, X.S. Zhao, Int. J. Hydrogen Energy 37 (2012) 19–30.
[26] A. Borodzinski, M. Bonarowska, Langmuir 13 (1997) 5613–5620.
[27] S. Jin, Z. Xiao, C. Li, X. Chen, L. Wang, J. Xing, W. Li, C. Liang, Catal. Today 234 (2014) 125–132.
[28] W.-S. Lee, A. Kumar, Z. Wang, A. Bhan, ACS Catal. 4104 (-) (2015) 4114.
[29] H. Yang, H. Gao, R.J. Angelici, Organometallics 19 (4) (2000) 622–629.
[30] R.A. Van Santen, Acc. Chem. Res. 42 (1) (2009) 57–66.
[31] H. Liu, W. Wang, X. Zhang, Y. Yang, K. Zhang, H. Peng, H. Luo, React. Kinet. Mech. Catal. 109 (2013) 537–549.